Estuaries and Coasts Vol. 30, No. 2, p. 296–310 April 2007

A Nearshore Model to Investigate the Effects of Seagrass Bed Geometry on Wave Attenuation and Suspended Sediment Transport

SHIH-NAN CHEN[1,*], LAWRENCE P. SANFORD[1], EVAMARIA W. KOCH[1], FENGYAN SHI[2], and ELIZABETH W. NORTH[1]

[1] *Horn Point Laboratory, University of Maryland Center for Environmental Science, Post Office Box 775, Cambridge, Maryland 21613*
[2] *Center for Applied Coastal Research, University of Delaware, Newark, Delaware 19716*

ABSTRACT: The effects of seagrass bed geometry on wave attenuation and suspended sediment transport were investigated using a modified Nearshore Community Model (NearCoM). The model was enhanced to account for cohesive sediment erosion and deposition, sediment transport, combined wave and current shear stresses, and seagrass effects on drag. Expressions for seagrass drag as a function of seagrass shoot density and canopy height were derived from published flume studies of model vegetation. The predicted reduction of volume flux for steady flow through a bed agreed reasonably well with a separate flume study. Predicted wave attenuation qualitatively captured seasonal patterns observed in the field: wave attenuation peaked during the flowering season and decreased as shoot density and canopy height decreased. Model scenarios with idealized bathymetries demonstrated that, when wave orbital velocities and the seagrass canopy interact, increasing seagrass bed width in the direction of wave propagation results in higher wave attenuation, and increasing incoming wave height results in higher relative wave attenuation. The model also predicted lower skin friction, reduced erosion rates, and higher bottom sediment accumulation within and behind the bed. Reduced erosion rates within seagrass beds have been reported, but reductions in stress behind the bed require further studies for verification. Model results suggest that the mechanism of sediment trapping by seagrass beds is more complex than reduced erosion rates alone; it also requires suspended sediment sources outside of the bed and horizontal transport into the bed.

Introduction

Deciphering the effects of seagrasses on water and sediments has been an active and challenging research area. Previous work has focused on the role of seagrass in reducing flow speed (Fonseca et al. 1982; Fonseca and Fisher 1986; Gambi et al. 1990; Koch 1993; Rybicki et al. 1997), modifying flow and turbulence structure (Ackerman and Okubo 1993; Nepf 1999; Ghisalberti and Nepf 2002; Abdelrhman 2003; Ghisalberti and Nepf 2004), altering sediment geochemical characteristics (Scoffin 1970; Wanless 1981; Wigand et al. 1997), attenuating wave energy (Fonseca and Cahalan 1992; Koch 1996; Kobayashi et al. 1993; Mendez et al. 1999), and affecting sediment dynamics (Ward et al. 1984; Almasi et al. 1987; Lopez and Garcia 1998; Gacia et al. 1999; Gacia and Duarte 2001). Recently, integration of the above perspectives has received increasing attention (Koch et al. 2006). Numerical models may help address the complex nature of this problem.

Teeter et al. (2001) review the physical, biological, and sedimentological complexities involved in constructing a complete wave-flow-seagrass-sediment model and present relevant equations as a point of departure. Teeter et al. state that the primary limitations on developing such a model are computational power and information on frictional damping of flow by seagrass blades and bottom sheltering effects on sediment resuspension by seagrass beds. Wave and flow damping by aquatic vegetation has been the focus of several recent modeling studies. These studies have focused on development of expressions and parameterizations for 1-dimensional or 2-dimensional frictional drag, in terms of a vegetation Reynolds number or canopy height and vegetation density. The drag force of the vegetation on waves or steady currents is usually expressed as

$$F = \frac{1}{2}\rho \bar{f} a u_b^2 \quad \text{or} \quad F = \rho C_d a U^2 \tag{1}$$

where F is force per volume, ρ is density, a is projected area perpendicular to the flow direction per unit water volume, $\bar{f}$ and C_d are the bulk drag coefficients for waves and steady currents, respectively, u_b is the amplitude of the wave induced velocity just above the bottom, and U is the steady current speed at some reference height (depth-

* Corresponding author; tele: 410/221-8296; fax: 410/221-8213; e-mail: schen@hpl.umces.edu

averaged velocity here). For purposes of comparison, the different approaches in the literature to estimating the bulk drag of seagrass may be categorized as Kobayashi-type models (Kobayashi et al. 1993; Mendez et al. 1999; Mendez and Losada 2004) and Nepf-type models (Nepf 1999; Ghisalberti and Nepf 2004).

Kobayashi et al. (1993) presented an analytical solution of wave height decay through vegetation based on linear wave theory, a Reynolds number dependent drag parameterization, and constant depth. The projected area per unit volume $a = N \times b_v$, where $N =$ the number of shoots per unit bottom area and b_v is defined as the plant area per unit height. Kobayashi et al. compared their model to flume studies on artificial kelp stands with $N = 1{,}100$ and 1,490 m^{-2}, and $b_v = 5.2\ 10^{-2}$ m, yielding $a = 57.2$ and 77.5 m^{-1}, respectively. The flume studies consisted of 60 runs with varying water depths (0.45–0.52 m), wave periods (0.714–2.0 s), and wave heights (0.036–0.1934 m). They used the bulk drag coefficient ($\overline{f}$) to calibrate the model for 60 runs and then correlated $\overline{f}$ with Reynolds number ($R = Ud/v$, where v is the kinematic viscosity of the water). They found that $\overline{f}$ decreases with increasing Reynolds number, and the relationship can be approximated by

$$\overline{f} = 0.08 + \left(\frac{2200}{R}\right)^{2.4} \tag{2}$$

Mendez et al. (1999) and Mendez and Losada (2004) expanded Kobayashi's solution by including swaying motion of the seagrass, wave breaking, and variable depth, and parameterized their model based on careful flume experiments. They allowed for swaying motion of the seagrass by changing the characteristic velocity in Eq. 1 to the relative velocity between plant and water. They reported another empirical relationship between bulk drag and Reynolds number:

$$\overline{f} = 0.4 + \left(\frac{4600}{R}\right)^{2.9} \tag{3}$$

Given the same Reynolds number, the bulk drag coefficient in Mendez et al. (1999) is higher than that in Kobayashi et al. (1993), because a lower velocity relative to the plant, when accounting for plant motion, requires a higher drag coefficient to maintain the same amount of wave energy attenuation. Their model fit to the data has a better correlation coefficient than Kobayashi et al.'s model. This suggests that the swaying motion of plants might need to be considered for optimal drag estimation.

Nepf (1999) used a different approach to explore the drag of vegetation on steady currents. She ignored the flexibility of the vegetation, mimicking the seagrass shoots using arrays of cylinders (width $d = 6.4$ mm). The projected area $a = nd$, where n is the number of shoots per unit bottom area and d is a typical shoot diameter; this definition of a is equivalent to the Kobayashi-type models. Based on observations for pairs of cylinders by Bokaian and Geoola (1984), she assumed that the bulk drag coefficient is a function of vegetation density as represented by the fractional volume occupied (ad). Numerical simulations were performed for both random and staggered arrays of cylinders with different element spacings (i.e., different values of ad). She showed that the bulk drag coefficient is relatively constant for ad up to 0.01 and declines steadily beyond this density (Fig. 6 in Nepf 1999). In the density-independent range ($0.001 < ad < 0.01$), the spacing between cylinders is too large for the wake behind an upstream cylinder to influence the drag of a downstream cylinder. In the steady-decline range ($0.01 < ad < 0.1$), the drag coefficient decreases due to turbulent wake interference that delays the point of separation on a downstream cylinder and subsequently leads to a lower drag (Kundu and Cohen 2002). In this model $\overline{f}$ was argued to be a weak function of Reynolds number.

Ghisalberti and Nepf (2004) considered the effects of canopy submergence on flow, turbulence, and drag. They found a significant reduction in drag relative to the Nepf (1999) expression when the top of the canopy was submerged, attributed to vortex shedding by the free end of the submerged grass blades. The bulk drag coefficient was approximately 64% of its value for emergent plants, depending weakly on the depth of the shear layer inside the canopy. They did not explore the effects of changing the degree of submergence. All of their experiments were carried out with canopy heights set at 30% of the water depth.

There are two main differences between these two types of models. Kobayashi-type models are for oscillatory flow (waves) while Nepf-type models are for steady currents. The Reynolds numbers are different as the characteristic velocities are wave orbital velocity and uniform current speed, respectively. In Kobayashi-type models the bulk drag is a function of Reynolds number that reflects the nature of the flow around a single shoot of vegetation. The bulk drag in Nepf's model is a function of density that reflects the properties of the whole bed.

All of these studies were vertically 2-dimensional, measuring or modeling a vertical slice through a grass bed in the direction of wave propagation or flow, with flow prevented from diverging around the

bed. While they were all instructive and valuable, they did not consider spatially varying seagrass bed geometry (e.g., less than complete seagrass coverage), spatially varying shorelines and bathymetries, or combinations of waves and currents. Although there have been several observational studies that indicate reduced sediment resuspension in seagrass beds due to lower shear stresses and enhanced sediment deposition (Lopez and Garcia 1998; Gacia and Duarte 2001), there have been almost no modeling studies of sediment transport in seagrass beds.

The model described by Teeter et al. (2001), as implemented at least partially in Teeter (2001), is an exception. It is quite comprehensive, including wind forcing, wave forcing, seagrass-enhanced drag, and sediment transport, but it depends extensively on empirical parameterizations based on local observations. Teeter (2001) implemented this model for Laguna Madre, Texas, representing vegetation drag by a fixed roughness (Nikuradse sand grain roughness $k_n \sim 0.2$ m), which was tuned to give reasonable agreement with field observations, but is not applicable to seagrass beds in other locations with other combinations of waves and currents.

We have developed a new, more flexible, approach for modeling interactions between waves, currents, and sediment transport in seagrass systems. The new model reduces the empiricism of the Teeter et al. (2001) approach by estimating wave and current drag that depends on seagrass density and height, based on Nepf (1999). It also considers 3-dimensional spatial variability in bed geometry and bathymetry, allows for both wave and current influences, considers the nearshore currents generated by wave breaking, calculates total bottom shear stress based on vector addition of wave and current stresses, and estimates fine sediment resuspension, deposition, and transport in and near seagrass beds. In the remainder of this paper, we describe the model development with an emphasis on drag estimation, validate it against flume studies of flow reduction by Gambi et al. (1990) and against field observations of wave damping, and present several model scenarios exploring the effects of seagrass bed geometries on wave attenuation, tidal current modification, and sediment trapping.

Methods

Numerical Modeling of Waves and Currents

We adapted the Nearshore Community Model (NearCoM) system and integrated a curvilinear nearshore circulation model SHORECIRC (Shi et al. 2003) and a wave driver REF/DIF-1 (Kirby et al. 2005) into the system. NearCoM aims to predict waves, circulations, and sediment transport in the nearshore ocean. SHORECIRC numerically solves the depth-integrated 2-dimensional horizontal equations and incorporates a semi-analytical solution for the vertical current profile (Svendsen et al. 2000). REF/DIF-1 accounts for shoaling, refraction, energy dissipation, and diffraction as waves propagate over variable bathymetry and determines short-wave forcing to drive currents in SHORECIRC. Our enhancements to the system include estimating seagrass effects on drag and turbulence, calculating the vector sum of wave and current bottom stresses, and adding a fine sediment transport module.

Seagrass Effects on Drag

For the model presented here, we adopted and modified the vegetation form drag expression of Nepf (1999), which was developed based on laboratory experiments with steady flows through rigid seagrass mimics. The primary reason for using this expression is that it explicitly accounts for the effects of seagrass shoot density over a realistic range of densities. The dominant seagrass species in the field studies to which we compare our model predictions was *Ruppia maritima* (leaf width $\sim$ 1.5 mm), with a fractional volume (ad) that fluctuated seasonally between about 0.0014 and 0.003. This range of ad is within the density-independent regime of Nepf (1999), but it is three orders of magnitude smaller than the values reported in Kobayashi et al. (1993) and Mendez et al. (1999) for their laboratory studies of seagrass wave drag. We apply the Nepf (1999) approach because we prefer to use steady flow drag data in comparable seagrass densities rather than wave drag data from a much higher seagrass density, and because we use the same basic drag formulation for both steady flow and wave forcing in our model.

Bottom shear stress (τ_{cs}) for steady currents is written using a standard quadratic law:

$$\tau_{cs} = \rho C_d U^2 \tag{4}$$

where ρ is flow density, U is depth-averaged flow velocity, and C_d is the drag coefficient. Assuming that seagrass blades may be modeled as rigid cylinders, Nepf (1999) partitioned total drag into skin friction due to the bottom stress at the sediment-water interface and form drag by the seagrass blades. She expressed the drag coefficient as

$$C_d = (1 - ad)\, C_B + \frac{1}{2}\overline{C_D} ad \left(\frac{h}{d}\right) \tag{5}$$

where a is the projected plant area per unit volume, d is shoot diameter, h is water depth, ad represents the fractional volume occupied by seagrasses, C_B is a skin friction drag coefficient (set equal to 0.001

here), and $\overline{C_D}$ is the bulk drag coefficient for seagrass, which Nepf (1999) determined from experiments. The first term on the right-hand side of Eq. 5 represents skin friction, whereas the second term represents form drag. We modified her calculation of a to allow seagrasses to only occupy part of the water column, so $a = nld/h$, where n is the number of seagrass shoots per unit area and l is the canopy height. Rearranging Eq. 5, the drag coefficient for current becomes

$$C_d = (1 - \frac{nld^2}{h}) C_B + \frac{1}{2}\overline{C_D}(nhd)(\frac{l}{h}) \tag{6}$$

C_d is a function of canopy height, shoot density, shoot diameter, and water depth. In Nepf (1999)'s model, $\overline{C_D}$ is a function of fractional volume (ad). We approximate the curve in Fig. 6 of Nepf (1999) as

$$\begin{aligned} \overline{C_D} &\approx 1.17, \quad 10^{-3} < ad < 10^{-2} \\ &\quad -0.255 \ln(ad), \quad 10^{-2} < ad < 10^{-1} \end{aligned} \tag{7}$$

Nepf (1999)'s model is for an emergent canopy. We account for submergence by scaling the form drag by the ratio of the canopy height to the water depth. A further reduction in drag may be needed to account for free-end effects at the top of submerged canopies (Ghisalberti and Nepf 2004). We have not made any additional modification to the Nepf (1999) expression because the experiments of Ghisalberti and Nepf were limited to deeply submerged canopies. It is reasonable to expect that the drag reduction they observed would be less for a less submerged canopy, but there is no data on the effects of different depths of submersion. Equation 6 is adopted as a reasonable starting approximation, pending additional data.

In Nepf's experiments the velocity was measured at 7.5 cm above the bottom, whereas the reference height in SHORECIRC is set at 1 m, requiring conversion of her drag coefficient to one that is relevant for SHORECIRC. SHORECIRC treats all drag as if it were generated by bottom boundary layer turbulence (Eq. 4). Although Nepf's expression (Eqs. 5 and 6) only assumes that a small part of the drag is generated by bottom boundary layer turbulence, the form of her total drag coefficient is operationally the same as for bottom boundary layer drag. We make the required conversion by assuming a logarithmic turbulent bottom boundary layer velocity profile and solving for a bottom roughness coefficient z_0 consistent with C_d from Eq. 6 at a reference height of $z = 7.5$ cm. Using this value of z_0 and a new reference height $z = 1$ m, we calculate the tidal current drag coefficient for SHORECIRC as

$$C_d = [\frac{k}{\ln(\frac{z}{z_0})}]^2 \tag{8}$$

where $k = 0.4$, the von Karman constant. This does not mean that the velocity profile within an actual grass bed is logarithmic. A recently study by Ghisalberti and Nepf (2002) shows that the flow structure within and just above an unconfined canopy resembles a mixing layer rather than a boundary layer. Resolving the vertical structure of the flow in the grass bed is beyond the scope of our study; we only want to parameterize the drag of the bed on the flow, for which purpose our approach is a reasonable approximation.

We used field observations to determine the seagrass bulk drag for waves in REF/DIF-1. Bottom shear stress due to pure wave action (τ_w) is expressed in terms of the wave friction factor (f):

$$\tau_w = \frac{1}{2}\rho f u_b^2 \tag{9}$$

where

$$f = (1 - ad) f_B + \frac{1}{2}\overline{f}\, ad(\frac{h}{d}) \tag{10}$$

where u_b is wave orbital velocity near the bottom, f_B is the wave skin friction factor, and $\overline{f}$ is a bulk drag representing the effects of seagrasses on waves. f_B was calculated using a bottom roughness equivalent to the value of $C_B = 0.001$ used in SHORECIRC, following procedures in U.S. Army Corps of Engineers (2002), while $\overline{f}$ was determined using field observations and assuming the functional form of Eq. 7 with an adjustable multiplicative coefficient (see below). As in Eq. 6, f depends on the ratio of canopy height to water depth (l/h) through the fractional volume ($ad = nd^2 l/h$).

Combining Wave and Current Bottom Stresses

Once the drag coefficient and wave friction factors are estimated through Eqs. 6 and 10, current and wave fields are calculated by SHORECIRC and REF/DIF-1. With this updated current and wave field (wave height and period) and with known bottom sediment grain size, skin friction shear stress due to pure current (τ_{cs}) and wave motions (τ_{ws}) are obtained using the techniques in U.S. Army Corps of Engineers (2002). Then we apply vector summation of the two skin friction components to calculate maximum skin friction shear stress (τ_{ms}):

$$\tau_{ms} = \sqrt{(\tau_{ws} + \tau_{cs}|\cos\phi_{wc}|)^2 + (\tau_{cs}\sin\phi_{wc})^2} \tag{11}$$

where ϕ_{wc} is the angle between current and wave

propagation and can be calculated from SHORECIRC and REF/DIF-1. Because we are interested in the maximum potential for sediment movement, the absolute value of $\cos\phi_{wc}$ is used in Eq. 11 to guarantee maximum vector summation regardless of the direction of wave orbital motion. This vector summation ignores enhanced turbulence due to nonlinear wave-current interactions in the bottom boundary layer (Grant and Madsen 1979). Given the high uncertainty of seagrass drag estimation and turbulence structure in seagrass beds, Eq. 11 is a reasonable first order approximation for combined wave-current bottom stress.

Sediment Transport Modeling

We developed and incorporated a suspended sediment transport module based on North et al. (2004). The module accounts for erosion and deposition with a simple parameterization of consolidation for single grain size cohesive sediments. We solve for changes in bottom sediment per unit area (B in kg m^{-2}) over time t at each grid point using

$$\frac{dB}{dt} = D - E - \gamma B \tag{12}$$

where D and E are the deposition and erosion rate (kg m^{-2}s^{-1}), respectively, and γ is a first order consolidation rate (s^{-1}; set equal to zero here). The formulation states that the amount of erodible sediment per unit area increases by deposition but decreases by erosion and consolidation. The deposition rate is calculated as

$$D = W_s C \tag{13}$$

where the settling velocity (W_s) is equal to 0.03 cm s^{-1} (a typical value for fine suspended sediment in Chesapeake Bay; Sanford et al. 2001) and C is depth-averaged suspended sediment concentration (kg m^{-3}). The erosion rate may be expressed as

$$E = M\left(\frac{\tau_{ms}}{\tau_c} - 1\right)\tilde{H}(\tau_{ms} - \tau_c)\tilde{H}\left(B + 2\frac{dB}{dt}\right) \tag{14}$$

where τ_c is critical shear stress for erosion (e.g., 0.15 Pa for fine sand), M is an empirical constant (5×10^{-5} kg m^{-2} s^{-1} here), and $\tilde{H}$ is the Heaviside step function ($\tilde{H} = 1$ when its argument is > 0 and $\tilde{H} = 0$ when its argument is ≤ 0). The first step function in Eq. 14 represents the initiation of sediment motion when the maximum bottom shear stress exceeds the critical value, while the second step function prevents over-erosion and negative values of B.

Given the erosion and deposition rates in each model cell, a third-order accurate numerical scheme QUICKEST (Leonard 1979) is used to solve the depth-averaged transport equation for suspended sediments (Clarke and Elliot 1998):

$$\frac{\partial(hC)}{\partial t} + \frac{\partial(hUC)}{\partial x} + \frac{\partial(hVC)}{\partial y} = \frac{\partial}{\partial x}\left(hK_x\frac{\partial C}{\partial x}\right) + \frac{\partial}{\partial y}\left(hK_y\frac{\partial C}{\partial y}\right) + E - D \tag{15}$$

where h is water depth, U and V are depth-averaged velocity components, and K_x and K_y are diffusion coefficients. The QUICKEST scheme reduces overshoot problems near strong gradients in concentration. This feature is particularly important because the presence of seagrass could lead to abrupt changes in bottom shear stress, which may in turn cause strong gradients in suspended sediment concentrations.

It should be noted that depth-averaged transport formulations used here effectively assume a vertically uniform sediment concentration profile. In reality, we expect sediment concentrations to be higher near the bottom, which can be approximately compensated for by increasing the value of W_s in Eq. 13. Different vertical profiles of turbulent mixing inside and outside the seagrass bed (Nepf and Vivoni 2000) would change the respective vertical profiles of suspended sediment concentration, slightly biasing the estimates of sediment deposition as a result. Because we intend to explore only first-order effects of seagrass beds on currents, waves, and sediments, depth-averaged transport formulations are adopted as a reasonable approximation.

Model Validation

Two model configurations were used for model validation. In the first, we set up the model to test the effects of seagrass under current-only conditions (using SHORECIRC only). Because we are particularly interested in modeling the effects of seagrass beds that cover only part of the model domain, such that water may flow around the bed rather than being forced through it or over it, we use the data of Gambi et al. (1990) for comparison. Gambi et al. studied flow speed reduction by *Zostera marina* L. (eelgrass, shoot diameter d = 0.28 cm) in a seawater flume, with the seagrass bed occupying only 20% of the width of the flume. SHORECIRC was configured to mimic the relative dimensions of their flume experiments. The actual model domain was considerably larger because of computational constraints, but the ratios of the domain length, domain width, and the horizontal extent of the eelgrass bed were scaled exactly (1 m seagrass bed length in the flume is scaled to 3,200 m in the

model). The canopy height was not scaled by the same factor; a canopy height of 0.75 m with 1 m water depth was used to mimic the flume bed and give a realistic drag coefficient. This does not affect the model-data comparison because we are interested only in the scaled horizontal structure of the flow field. Flow was driven using an upstream flux boundary condition, with no flow through the domain sidewalls, to generate the same free-stream velocities as Gambi et al. The eelgrass parameters they reported were used to calculate the drag coefficient for SHORECIRC based on Eqs. 6 and 7. We computed the volume flux reduction within the eelgrass bed from just upstream of the bed to the end of bed where flow reached a steady condition. The volume flux reduction is defined as

$$(1 - \int Udz / \int U_{control}\, dz) \times 100 \tag{16}$$

where $U_{control}$ is the up-stream velocity. We choose combinations of two shoot densities (600 and 1,200 shoots m^{-2}) and two free-stream velocities (10 and 20 cm s^{-1}). Comparisons are shown in Fig. 1. The model-predicted values for the four different combinations agree reasonably well with Gambi et al.'s results, without any parameter tuning. As expected, the eelgrass bed with higher shoot density results in higher volume flux reductions. The model-predicted volume flux reduction increases rapidly behind the leading edge of the eelgrass bed and levels off approximately halfway into the bed.

In the second model validation exercise, the model was configured to test the effects of seagrass on wave attenuation (using RED/DIF-1 only). We used field observations to determine the magnitude of the wave form drag, because equivalent data to that of Nepf (1999) on the relationship between seagrass density and wave form drag ($\bar{f}$) is not available. The field observations were carried out in Duck Point Cove, near Bishop's Head Point, Maryland, in mesohaline Chesapeake Bay (Newell and Koch 2004). A time series of wave height and seagrass parameters were measured in different months at two adjacent sites parallel to the shoreline, one vegetated with *R. maritima* and the other unvegetated. The size of *R. maritima* bed was about 600 m in the alongshore direction and 200 m in the crossshore direction, and a pressure sensor was located at the center in average water depth of 1 m. Assuming the same incident wave climates at the two sites, we can plot wave height measurements at the unvegetated site against the vegetated site to evaluate wave attenuation by the *R. maritima* bed. Assuming that $\bar{f}$ is a function of fractional volume (ad) and has similar functional form to that for steady current (Eq. 7), we change the height of the $\bar{f}$ curve to obtain the observed wave attenuations in October. The calibrated $\bar{f}$ is written as

$$\begin{aligned} \bar{f} &\approx 0.253, \quad 10^{-3} < ad < 10^{-2} \\ &\quad -0.055 \ln(ad), \quad 10^{-2} < ad < 10^{-1} \end{aligned} \tag{17}$$

We validated the October-derived calibration by applying observed seagrass parameters for May and June, then calculating the corresponding wave friction factors and comparing the model-predicted wave heights with observations. Table 1 summarizes the slopes and goodness of linear fits from the field observations and the calibrated model. A slope less than 1 indicates wave attenuation. Both the October calibration run and May validation run slopes agree well with the data, which show mild wave attenuation. Wave attenuation by the seagrass bed peaked in June when the seagrass canopy occupied the whole water column. The model qualitatively captures this trend (June attenuation > May and October) although the model tends to slightly underestimate wave attenuation in June.

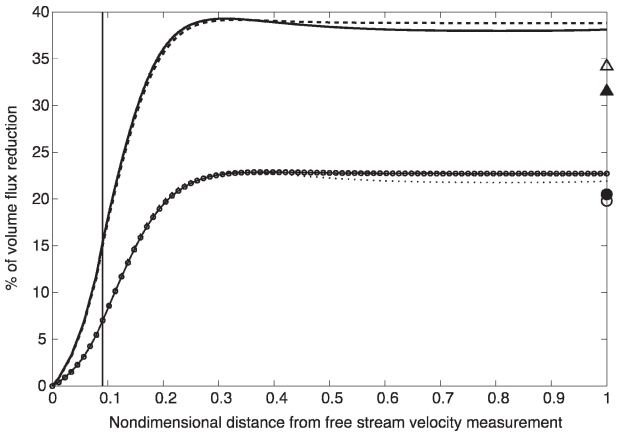

Fig. 1. Comparison of flow speed reduction in a seagrass bed between the model prediction (4 curves) and flume data (4 discrete points: 2 triangles and 2 circles) reported by Gambi et al. (1990). The percentage of volume flux reduction is used as an indicator of flow speed reduction and is plotted against the relative distance beyond (downstream of) the free-stream velocity measurements. Relative distance is normalized by the distance between the free-stream measurement and the end of the bed. The leading edge of the seagrass bed is indicated by the vertical line. The solid and dashed curves are model predictions for shoot density 1,200 m^{-2} with 10 and 20 cm s^{-1} free-stream velocity, respectively. The dotted and circle curves are model predictions for shoot density 600 m^{-2} with 10 and 20 cm s^{-1} free-stream velocity, respectively. The solid and open triangles represent Gambi et al.'s results for shoot density 1,200 m^{-2} with 10 and 20 cm s^{-1} free-stream velocities, respectively, whereas the solid and open circles are Gambi et al.'s results for 600 m^{-2} with 10 and 20 cm s^{-1}.

TABLE 1. Linear fits (zero intercept) of unvegetated (x axis) versus vegetated (y axis) wave heights from field observations, for comparison to the calibrated model in May, June, and October, 2001.

	May		June		October	
	Slope	R^2	Slope	R^2	Slope	R^2
Observation	0.97	0.84	0.75	0.81	0.95	0.96
Model	0.95	–	0.88	–	0.92	–

This approach has the advantage that a wider range of vegetation density is covered with one empirical parameter ($\bar{f}$). This is particularly useful for simulating seasonally or geographically varying seagrass populations. The underestimation of wave attenuation in June may be due to a different response to oscillatory forcing, the flexibility of real seagrass blades (i.e., in June the reproductive stems may have different flexibility from the vegetative stems in other months), a Reynolds number dependence for which we have not accounted, or additional drag force due to sediment bed forms. The drag partitioning for current and waves here assumes a flat sediment bed due to a lack of field measurements on bed forms. Further study is needed to understand the influence of these effects, and a wide range of realistic vegetation densities, on the bulk drag of seagrass. For the present purpose, the qualitative reproduction of changing wave drag due to seasonal changes in seagrass morphology is considered sufficient.

Model Setup and Scenarios

The model domain is set at 720 m in the shore-normal direction and 5,400 m in the shore-parallel direction with a 10 × 30 m grid resolution. Two bathymetries are set up: a flat bottom with 1 m depth and a sloping bottom with 2.5 m depth offshore and 0.05 m depth at the shoreline. When present, tidal currents are assumed to be primarily in shore-parallel direction with a maximum magnitude of about 20 cm s^{-1}. Tidal currents are simulated by imposing flux boundary conditions through the upstream and downstream boundaries of the domain at semidiurnal frequency. A 4-s sinusoidal wave enters the domain from the offshore boundary with wave heights varying between 0.1 and 0.4 m, at an incident angle of either 0° (scenarios 1–3) or 10° (scenario 4) counterclockwise from the shore-normal direction. The domain of the sediment module is smaller than the entire SHORECIRC/REFDIF-1 domain to avoid anomalous physical forcing near the boundaries, and a looping boundary condition is applied in the shore-parallel direction so that the sediment flux leaving one end of the domain equals the flux entering the other end of the domain. Bottom sediments are initialized with $B = 3$ kg m^{-2} uniformly distributed throughout the domain. This avoids depletion of the bottom sediment supply over the duration of a run and the corresponding additional complexity. In addition to the scenarios reported here, the sediment transport module was verified to conserve mass when suspended sediments and bottom sediments are totaled.

Model scenarios were designed to investigate the effects of seagrass bed geometry on wave transformations and sediment transport. Model scenarios include three flat bottom cases with varying width, length, and position of the seagrass bed and one sloping bottom case with three different bed geometries (Table 2). The seagrass parameters observed in June for *R. maritima* are applied (density is 1,270 m^{-2}; canopy height is 1 m). The circulation, wave, and sediment modules are turned on in all scenarios, and we look at several output quantities.

The first two scenarios examine the effect of seagrass bed width and alongshore extents on reduction of the wave energy flux reaching the shoreline. Wave energy flux (F) is the rate at which wave energy is transported in the horizontal direction and can be expressed as

$$F = EC_g = \left(\frac{1}{8}\rho g H^2\right) C_g \tag{18}$$

where E is the wave energy density, C_g is group velocity, ρ is water density, g is the gravitational constant, and H is wave height. In these two scenarios, we change the geometry of the seagrass bed and calculate the ratio of F with and without seagrasses, averaged over the entire shoreline. The percentage of wave energy flux reduction is then $(1 - F_{with}/F_{without}) \times 100$.

The third scenario examines the effect of seagrass bed location (distance offshore) on reduction of bottom stress over the total domain. Because we are interested in the influences of the seagrass bed on the total force acting on the bottom sediments in the domain, we define the total bottom stress as the skin friction shear stress integrated over the whole domain. The ratio of total bottom stress with and without the seagrass bed is used to calculate the percentage reduction. In the third scenario, the percent bottom stress reduction is compared as the mid point of the bed is moved from an inshore position toward the offshore boundary, with bed width and length fixed.

TABLE 2. Model scenarios.

Scenario	Bathymetry	Crosshore bed width (m)	Alongshore bed length (m)	Position	Output quantities
1	Flat (1 m)	0 to 700 (50-m intervals)	Full alongshore domain	Offshore edge of the bed fixed at the offshore boundary	Percent of wave energy flux reduction
2	Flat (1 m)	100	300 to full alongshore domain (300-m intervals)	Offshore edge of the bed fixed at the offshore boundary; Center of the bed fixed at the center of alongshore domain	Same as above
3	Flat (1 m)	100	Full alongshore domain	Center of the bed located 50 to 650 m from the offshore boundary (50-m intervals)	Percent of total bottom stress reduction
4	Sloping (2.5 m offshore, 0.05 m onshore)	0	0		Wave height and skin friction shear stress
		200	1,800	Center of the bed located 550 m from the offshore boundary	Same as above
		Full crosshore domain	1,800	Center of the bed located 360 m from the offshore boundary	Same as above

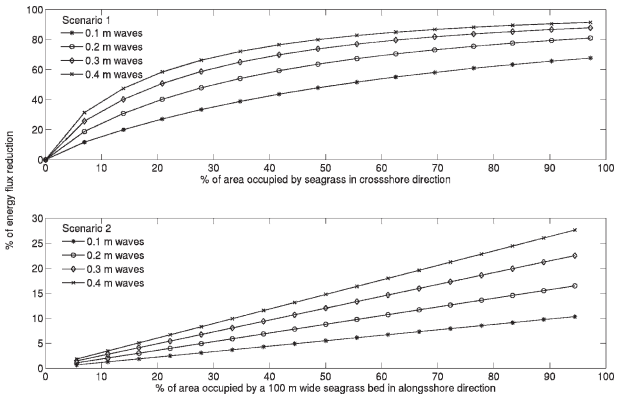

Fig. 2. Changes in wave energy flux reduction (indicator of wave attenuation) on the shoreline when the crossshore and alongshore seagrass bed width increases (see scenario 1 and 2 in Table 2 for details). Incident wave angles are zero degree (shore-normal direction). Seagrass parameters (shoot density and canopy height) in June were used.

The last scenario (with a sloping bottom) is more realistic than the constant depth scenarios. It examines the overall influence of seagrass presence and extent on tidal currents, waves, and sediment transport in more detail. We examine changes in wave height, skin friction shear stress, suspended sediment, and bottom sediment over both space and time through two tidal cycles. Cases considered are no seagrass, a seagrass bed of limited extent, and a seagrass bed covering the full domain.

Results

Larger seagrass bed width in the direction of wave propagation results in higher wave attenuation, and relative wave attenuation increases as incoming wave height increases. Figure 2 shows changes in wave energy flux reduction when the crossshore bed width is varied but the bed occupies the entire domain in the alongshore direction (scenario 1). The results are presented with respect to only the crossshore direction, since there is no alongshore variation. Wave energy flux reduction increases with crossshore width but levels off as maximum width is approached. The increase in energy flux reduction is obviously due to the increase in seagrass wave drag as the bed becomes wider. The energy flux reduction levels off at large bed width simply because not much wave energy is left to dissipate, so the rate of change decreases.

Percent energy flux reduction also increases with increasing wave height. This is because a larger wave height exerts a higher stress on the bottom, proportional to the wave orbital velocity squared. The wave energy dissipation rate is proportional to the product of stress and wave orbital velocity for rough turbulent flow (Dean and Dalrymple 1991),

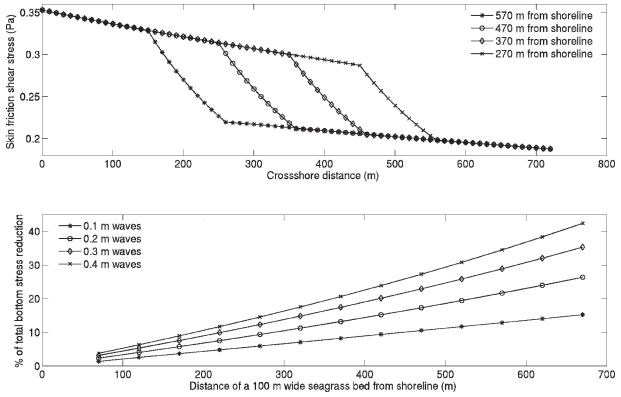

Fig. 3. Skin friction evolution when 0.2 m waves propagate along a central transect from the offshore boundary to shoreline (upper panel) and total bottom stress reduction (lower panel) when a seagrass bed is moved away from shoreline (scenario 3 in Table 2). Wave and seagrass parameters are the same as Fig. 2.

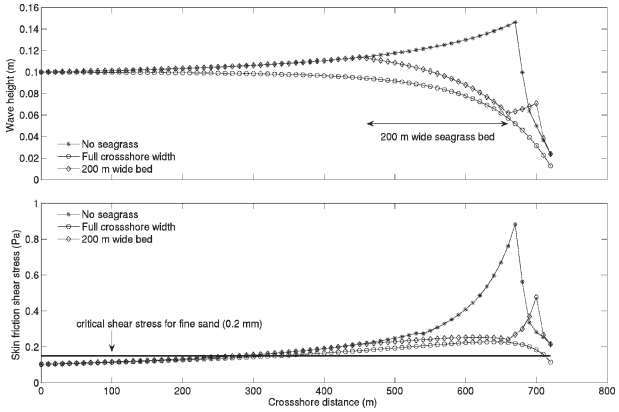

Fig. 4. Wave height evolution when waves propagate along a central transect from the offshore boundary to shoreline (upper panel) and the corresponding changes in skin friction shear stress (lower panel) under three seagrass bed configurations. See scenario 4 in Table 2 for details. Seagrass parameters in June were used.

so wave energy dissipation is proportional to orbital velocity (wave height) cubed, while wave energy flux is only proportional to wave height squared. Wave energy dissipation is proportionately more effective for higher waves.

Increasing seagrass bed length alongshore (perpendicular to wave propagation) linearly reduces the wave energy flux at the shoreline. Figure 2 shows changes in wave energy flux reduction on the shoreline for scenario 2, in which we change the alongshore length of the bed while keeping the crossshore width fixed. As expected, wave energy flux reduction is linearly proportional to the alongshore seagrass bed length. Again, percent energy flux reduction increases with incident wave height.

With fixed seagrass bed geometry and a flat bottom, moving the bed away from the shoreline reduces the total force exerted on the bottom. Figure 3 presents the skin friction distribution and the percent reduction in total force acting on bottom sediments as the position of the bed is moved from inshore towards the offshore boundary (scenario 3), with a fixed bed width of 100 m and length covering the whole domain in the alongshore direction. In the upper panel of Fig. 3, 0.2-m waves are applied in the shore-normal direction, and as the bed is moved toward the shoreline, the abrupt reduction in skin friction (indicating the area occupied by seagrass) is moved accordingly. It should be noted that the skin frictions at the shoreline for different bed locations are about the same. This may be due to very weak nonlinearities in wave energy dissipation in this flat bottom scenario and due to the absence of wave diffraction because the seagrass bed covers the entire alongshore domain. In the lower panel of Fig. 3, the percent of total bottom stress reduction is calculated according to the previous section. The total bottom stress with a seagrass bed is the integral average of skin friction distribution over the crossshore distance, as shown in Fig. 3. It can be seen that total bottom stress reduction increases approximately linearly with the offshore distance of the bed. It makes sense that total force acting on bottom sediments is reduced by moving the bed offshore because the affected area between the bed and shoreline increases linearly with the distance of the bed offshore. The smaller waves that emerge from the seagrass bed act over this entire area. Again, larger waves result in proportionately higher bottom stress reduction.

Seagrass bed geometry also influences sediment dynamics, in ways that are more complex than the reduction in bottom stress alone. In the fourth scenario, the more realistic sloping bottom case, we compare model runs with no seagrass, a seagrass bed 200-m wide and 1,800-m long, and a seagrass bed that covers the entire width of the domain and is 1,800-m long. Figure 4 shows crossshore transects of wave height and skin friction shear stress across the center of the seagrass bed at slack tide. In the upper panel of Fig. 4, wave shoaling and then breaking as waves propagate shoreward can be seen without the seagrass bed. This wave height evolution corresponds to the increase and quick drop of skin friction shear stress shown in the lower panel of Fig. 4. In both cases with seagrass beds, wave height and skin friction shear stress within and behind the bed are greatly reduced. The breaking zone and the peak of skin friction shear stress for the case with

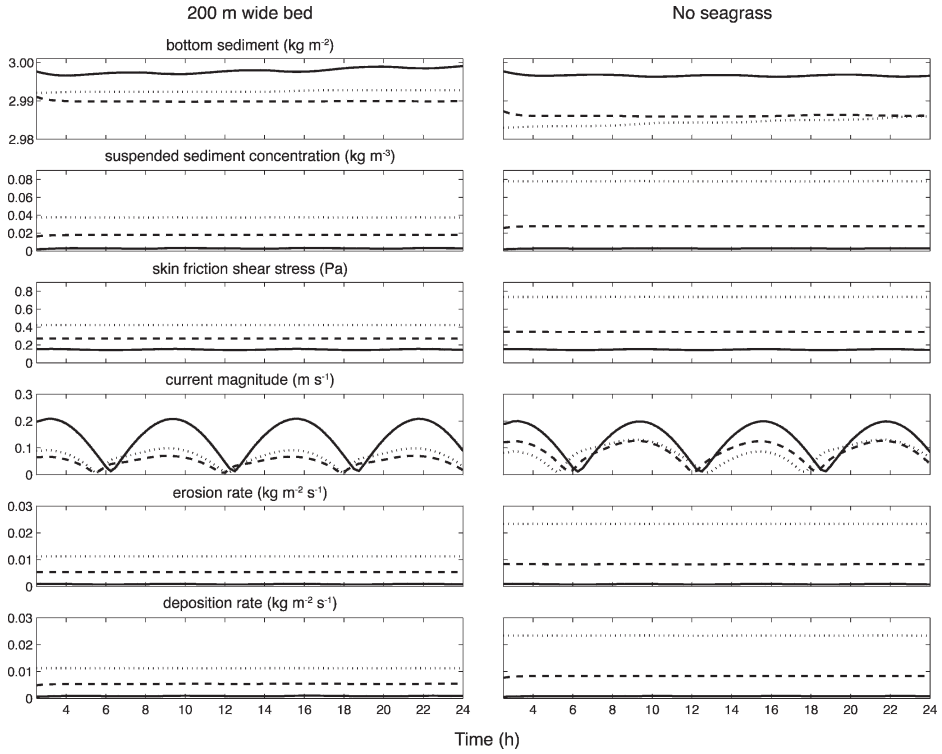

Fig. 5. Time series comparing a 200 m wide bed with a no seagrass case, as described in scenario 4. Predictions are from the central transect shown in Fig. 6. The solid line here represents the spatial average of each variable from the offshore boundary to the offshore edge of the bed (450 m from offshore boundary); the dashed line is the spatial average within the bed (from 450 to 650 m); the dotted line is the spatial average over the rest of the domain. Seagrass parameters in June were used.

a 200-m wide bed are moved shoreward. When the crossshore domain is fully occupied by the seagrass bed, the breaking zone disappears. Differences between all three cases in deeper water near the offshore boundary are relatively small. The reason is that short period wave orbital velocity decays with depth, making bottom friction less effective to dissipate wave energy in deeper areas. Interactions between seagrass beds and waves in deeper water depend on wave period; longer period waves interact more effectively with seagrass beds in deeper water.

Reduced skin friction has important implications from the standpoint of sediment transport. To demonstrate this, we put a line in Fig. 4 to indicate the critical shear stress (about 0.15 Pa; U.S. Army Corps of Engineers 2002) for fine sands (0.2 mm). Sediments start to move when shear stress exceeds a critical value (Eq. 14). As shown in Fig. 4, the distances over which the critical stress is exceeded are about the same with or without the seagrass beds. The erosion rate is proportional to the distance between the lines of wave-induced skin friction and critical shear stress (Eq. 14), so erosion rate is greatly reduced within and behind the seagrass beds. This implies that, without advection of sediment from external sources, suspended sediment concentrations within and behind the beds may be lower than those with no seagrass bed. Although greatly simplified, these model results illustrate that seagrass bed geometries can have profound effects on waves and can subsequently influence sediment dynamics.

To further examine the effects of seagrass beds on sediment dynamics, we compare the time series of six variables associated with sediments between the 200-m wide bed case and the no seagrass case (Fig. 5) over 2 full tidal cycles. The variables are bottom sediments, suspended sediment concentration, skin friction shear stress, current magnitude, erosion rate, and deposition rate. In Fig. 5, each panel contains three lines that represent the averaged values of each variable offshore of the bed, within the bed (or where the bed would be), and between the bed and the shoreline. As can be seen in Fig. 5, current magnitudes show semidiurnal tidal signals and, when the seagrass bed is not present, they decrease shoreward due to increased bottom friction. Current magnitudes at the onshore position during floods are slightly smaller than ebbs because flooding tides are against wave-induced alongshore currents (toward

positive y direction). When a 200-m wide bed is added, current magnitude inside the bed is reduced and becomes smaller than either offshore or onshore. Tidal signals are very weak in the other variables, especially for shallower locations, indicating that the sediment dynamics in the system are dominated by waves. Most importantly, averaged suspended sediment concentration, skin friction shear stress, erosion rate, and deposition rate are lower and there is more bottom sediment at both the seagrass bed and onshore positions when the seagrass bed is present. This result confirms the anticipation of lower suspended sediment concentration from Fig. 4 and suggests that seagrass beds can protect bottom sediments from being eroded not only inside the bed itself but also the area behind it.

The spatial distributions of predicted suspended and bottom sediments indicate that the mechanism of sediment trapping by seagrass beds requires not only reduced erosion but also a suspended sediment source outside the bed and horizontal transport into the bed. Figure 6 shows a snapshot of distributions of suspended (lower panels) and bottom sediments (upper panels) with and without the seagrass bed at maximum flood. For the no seagrass case, suspended sediment concentration increases shoreward with little alongshore variation, causing bottom sediments to decrease. This pattern again indicates the dominance of wave-induced erosion. Adding a 200-m wide seagrass bed induces both alongshore and crossshore variations of suspended and bottom sediment distributions, as can be seen in Fig. 6. Due to higher drag of the bed, tidal currents are forced to flow around it, resulting in a bulge of suspended sediments at the upstream offshore corner of the bed. A similar pattern is observed at the downstream offshore corner when tides change direction. In general, suspended sediment concentration within the bed is lower than that either onshore or offshore, but advection of suspended sediments by tidal currents can locally increase the concentration within the bed. As for bottom sediments, local scouring is evident at the corners of the bed on the nearshore side. The scouring could be due to enhanced tidal flow speed between the shoreline and the bed. We found no published field observations to support such scouring and suspect that this effect may be exaggerated by the wall boundary condition in the model. There are generally more bottom sediments within the bed than on either side, mostly near the upper and lower edges. The sediment trapping is due to import of higher suspended sediment concentration by tidal currents from outside, deposition of these sediments, and lower wave-induced erosion rates inside. Animating the model results confirms that sediment trapping appears to occur at the upstream edge on each half tidal cycle, when tidal currents are advecting higher suspended sediment concentrations from outside into the seagrass bed.

Discussion

Wave Attenuation by Seagrass Beds

Several general statements can be made from the results of the model scenarios with a flat bottom (Figs. 2–3). Larger seagrass bed width in the direction of wave propagation results in higher wave attenuation (indicated by percentage of energy flux reduction) and less energy on the shoreline. The total force acting on the bottom (indicated by percentage of bottom stress reduction) in the whole domain decreases as the seagrass bed is moved offshore. Relative wave attenuation and bottom stress reduction increase with incoming wave height.

These statements are generally valid as long as there is a significant interaction between wave orbital velocity and the seagrass canopy. This qualification may be interpreted as a generalization of suggestions by Ward et al. (1984), Fonseca and Cahalan (1992), and Koch (2001). They pointed out that wave attenuation should be higher when seagrass occupies a large portion of the water column. For the flat bottom cases, seagrass canopy occupied the entire water column (June case), and the decay of orbital velocity is negligible (at 1 m depth, 4 s waves are close to shallow water waves). In the sloping bottom case 1-m seagrass canopy only occupied part of the water column in the deepest region (2.5 m), and orbital velocity decayed at least 25%. This is why the differences in wave height (Fig. 4) between no seagrass and full crossshore width cases are relatively small at the deepest region but increasing toward shallower regions. Although a flume study (Fonseca and Cahalan 1992) and field observation (Koch 1996) indirectly support this hypothesis, wave attenuation has also been observed when seagrass only occupies a small portion of the water column (Granata et al. 2001 observations at a depth of 15 m). Systematic observations on the effects of seagrass bed geometry on waves with different wave heights and periods are needed to verify the model predictions and to better understand the processes.

Wave attenuation by seagrass may have implications for shoreline protection. A few authors have postulated that seagrass beds could reduce the energy that reaches shorelines, and potentially protect shorelines from being eroded (van Katwijk and Hermus 2000). Using the observed seagrass parameters of June, our model results show signif-

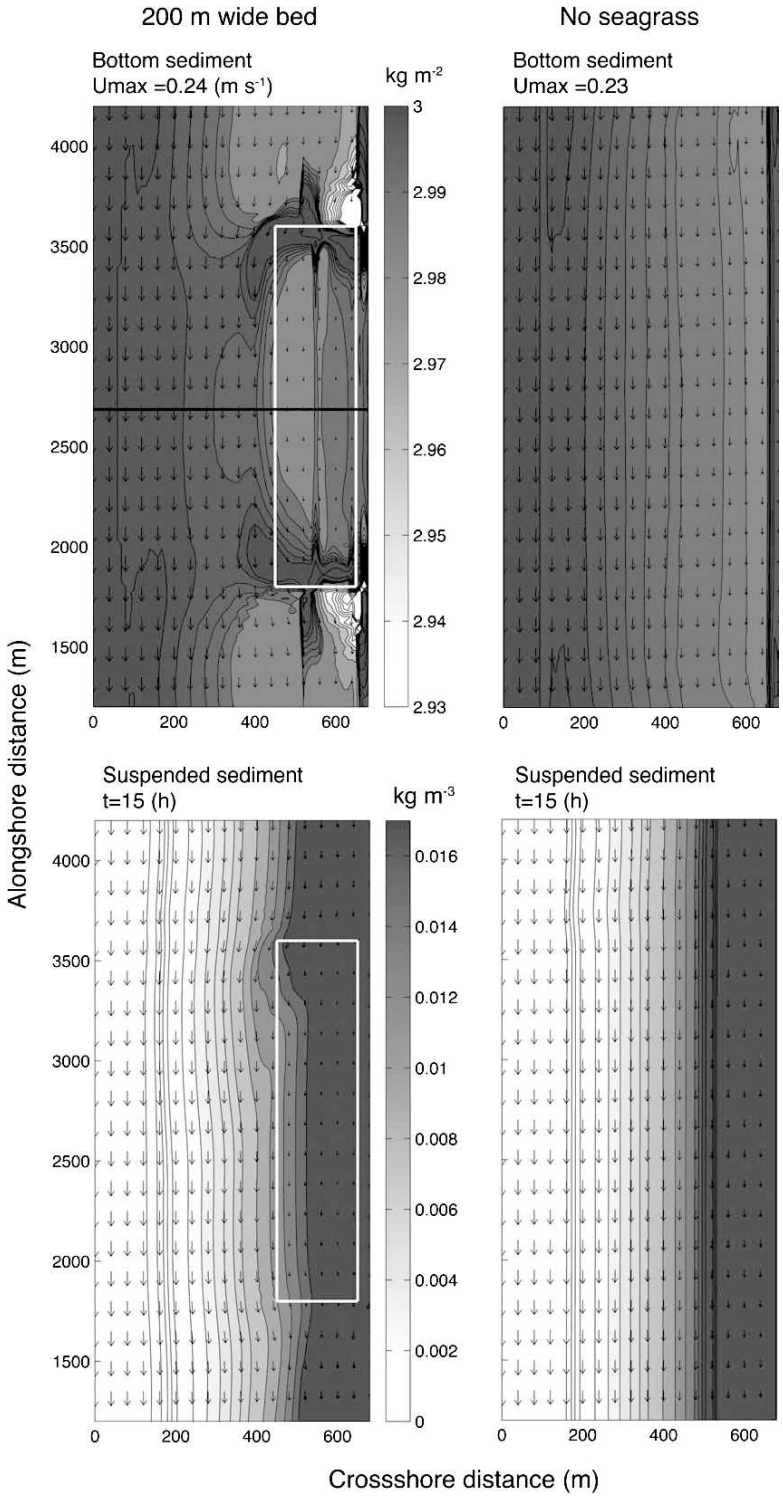

Fig. 6. Snapshot (top-view of model domain) of the distribution of bottom sediments (upper panels) and suspended sediment concentrations (bottom panels) comparing a 200 m wide bed with a no seagrass case. The M2 tide is forced in the along-shore direction, while 0.1 m, 4 s waves propagate from offshore boundary with 10 degree incident angle (counter-clockwise from shore-normal direction). The current direction and magnitude are indicated by vectors, and bottom sediment and suspended sediment concentrations are shown in the contours. Seagrass parameters in June were used.

icant reductions of wave energy flux at the shoreline in both the flat and sloping bottom scenarios (Figs. 2 and 4). Seagrass presence varies spatially, seasonally, and interannually in temperate environments, whereas shoreline erosion is usually associated with wave events that occur episodically (Wilcock et al. 1998) over annual or decadal time scales (Kamphuis 1987). Timing between wave events and seagrass growth probably influences the potential for seagrass beds to protect shorelines. Without knowing this timing, it is difficult to evaluate the net influence of seagrass on shoreline protection based on the results presented here. Other factors such as spectral or directional distributions of wave energy may need to be considered in order to better address this question. REF/DIF is capable of modeling spectral wave forcing as well as multiple wave incident angles (Kirby and Tuba Ozkan 1994) and will be addressed in the future.

Sediment Dynamics

Model results presented in this paper have two main implications for sediment dynamics. Sedimentary processes are altered within the seagrass bed and probably behind it. Results from scenario 3 (Fig. 3) show that, in wave-dominated environments, the total force acting on bottom sediments decreases as the seagrass bed is moved offshore due to increases in the affected area behind the bed. This suggests that seagrass beds may stabilize bottom sediments in the zone between the bed and shoreline, which is consistent with Hine et al. (1987)'s observation that disappearance of a seagrass community allowed rapid onshore and alongshore sand transport in the nearshore zone. Comparison between cases without and with a 200-m wide bed (Fig. 5) shows lower skin friction shear stress, lower erosion rate, and higher level of bottom sediments at locations within and behind the bed. Within the bed, our result is consistent with Lopez and Garcia (1998)'s findings of reduced shear stress and consequently lower suspended sediment transport (partly due to lower suspended sediment concentration) in the vegetated area. Reduced erosion rate as well as bottom sediment retention are also supported by field observations (Gacia and Duarte 2001). Gacia and Duarte found that the presence of *Posidonia oceanica* enhances sediment stability by preventing resuspension. Quantitative evidence does not exist to support the model-predicted reduction in skin friction shear stress and erosion and sediment retention between the bed and shoreline. Further studies are required for verification.

The second implication of our results for sediment dynamics stems from the 3-dimensional nature of our modeling approach: sediment trapping in the seagrass bed requires horizontal transport of suspended sediment from outside of the bed into the bed. The concept of the seagrass bed as a depositional environment has been suggested by several authors (e.g., Grady 1981; Ward et al. 1984; Almasi et al. 1987), and the proposed mechanism for this accumulation may be summarized as reduced shear stress due to loss of momentum in a seagrass bed leading to reduction in resuspension and increased sediment accumulation (Koch et al. 2006). This connection between lower momentum and reduced resuspension (lower erosion rate) is supported by our results. Our results also suggest that linkages from reduced resuspension to increased accumulation are not trivial and may not occur everywhere within the bed. Sediment accumulation at one location could occur when the suspended sediment concentration is high enough that the deposition rate exceeds the erosion rate. Sediment accumulation at the upper and lower edges of the bed in Fig. 6 illustrates this point. At these two edges, accumulation occurs when high concentrations of suspended sediments from outside are transported into the bed where reduced shear stresses allow deposition. The amount of accumulated sediments then gradually decreases with distance into the bed until the sediment source from outside is used up. Further into the bed, original sediments remain but there is no new accumulation. In short, the model results clearly demonstrate that sediment accumulation requires both sediment sources (outside the bed here) and a transport mechanism (tidal current here), both of which may vary spatially within the bed. The reduction in suspended sediment transport capacity (concentration multiplied by streamwise velocity) in a vegetated area reported by Lopez and Garcia (1998) indirectly supports accumulation at the bed edge. Direct observations on spatial patterns of accumulation within seagrass beds are few, and most of them focus on sediment grain size distributions (e.g., Scoffin 1970; Wanless 1981; Granata et al. 2001). It should be noted that the spatial distribution of bottom sediment presented here may not match field observations precisely because the model does not account for limited supplies of surficial sediments and mixed sediment grain sizes. More observations that resolve spatial patterns of erosion and deposition are needed to enhance our understanding of the interactions between seagrass, sediment, and the physics of nearshore environments.

Acknowledgments

This research was supported in part under award NA16RG2207/SA07-5-28051S from Maryland Sea Grant, National Oceanic and Atmospheric Administration, U.S. Department of

Commerce, by Cooperative Institute for Coastal and Estuarine Environmental Technology - CICEET (Grant No. W912HZ-05-C-0033), and by the U.S. Army Corps of Engineers (Contract No. 00-366). The statements, findings, conclusions, and recommendations are those of the authors and do not necessarily reflect the views of Maryland Sea Grant, the National Oceanic and Atmospheric Administration, or U.S. Department of Commerce. S. N. Chen was partially supported by a graduate fellowship from Horn Point Laboratory. We would like to thank Dr. James T. Kirby who made the Nearshore Community Model available to us. This is University of Maryland Center for Environmental Science publication no. 4077.

Literature Cited

Abdelrhman, M. A. 2003. Effects of eelgrass *Zostera marina* canopies on flow and transport. *Marine Ecological Progress Series* 248:67–83.

Ackerman, J. D. and A. Okubo. 1993. Reduced mixing in a marine macrophyte canopy. *Functional Ecology* 7:305–309.

Almasi, M. N., C. M. Hoskin, J. K. Reed, and J. Milo. 1987. Effects of natural and artificial *Thalassia testudinum* on rates of sedimentation. *Journal of Sedimentary Petrology* 57:901–906.

Bokaian, A. and F. Geoola. 1984. Wake-induced galloping of two interfering circular cylinders. *Journal of Fluid Mechanics* 146:383–415.

Clarke, S. and A. J. Elliott. 1998. Modelling suspended sediment concentration in the firth of forth. *Estuarine Coastal and Shelf Science* 47:235–250.

Dean, R. G. and R. A. Dalrymple. 1991. Water Wave Mechanics for Engineers and Scientists. 1st edition. World Scientific, Singapore.

Fonseca, M. S. and J. A. Cahalan. 1992. A preliminary evaluation of wave attenuation for four species of seagrass. *Estuarine Coastal and Shelf Science* 35:565–576.

Fonseca, M. S. and J. S. Fisher. 1986. A comparison of canopy friction and sediment movement between four species of seagrass with reference to their ecology and restoration. *Marine Ecology Progress Series* 29:15–22.

Fonseca, M. S., J. S. Fisher, J. C. Zieman, and G. W. Thayer. 1982. Influence of the seagrass, *Zostera marina*, on current flow. *Estuarine Coastal and Shelf Science* 15:351–364.

Gacia, E. and C. M. Duarte. 2001. Sediment retention by a Mediterranean *Posidonia oceanica* meadow: The balance between deposition and resuspension. *Estuarine Coastal and Shelf Science* 52:505–514.

Gacia, E., T. C. Granata, and C. M. Duarte. 1999. An approach to the measurement of particle flux and sediment retention within seagrass (*Posidonia oceanica*) meadows. *Aquatic Botany* 65:255–268.

Gambi, M. C., A. R. M. Nowell, and P. A. Jumar. 1990. Flume observations on flow dynamics in *Zostera marina* (eelgrass) beds. *Marine Ecology Progress Series* 61:159–169.

Ghisalberti, M. and H. M. Nepf. 2002. Mixing layers and coherent structures in vegetated aquatic flows. *Journal of Geophysical Research* 107:1–11.

Ghisalberti, M. and H. M. Nepf. 2004. The limited growth of vegetated shear layers. *Water Resources Research* 40:W07502.

Grady, J. R. 1981. Properties of seagrass and sand flat sediments from the intertidal zone of St. Andrew Bay, Florida. *Estuaries* 4: 335–344.

Granata, T. C., T. Serra, J. Colomer, X. Casamitjana, C. M. Duarte, and E. Gacia. 2001. Flow and particle distributions in a nearshore meadow before and after a storm. *Marine Ecology Progress Series* 218:95–106.

Grant, W. D. and O. S. Madsen. 1979. Combined wave and current interaction with a rough bottom. *Journal of Geophysical Research-Oceans and Atmospheres* 84:1797–1808.

Hine, A. C., M. W. Evans, R. A. Davis, and D. Belknap. 1987. Depositional response to seagrass mortality along a low-energy, barrier island coast: West-central Florida. *Journal of Sedimentary Petrology* 57:431–439.

Kamphuis, J. W. 1987. Recession rate of glacial till bluffs. *Journal of Waterway Port Coastal and Ocean Engineering-ASCE* 13:60–73.

Kirby, J. T., R. A. Dalrymple, and F. Shi. 2005. Combined refraction/diffraction model, REF/DIF 1, Version 3.0, Documentation and User's Manual, Research Report, Center for Applied Coastal Research. University of Delaware, Newark, Delaware.

Kirby, J. T. and H. Tuba Ozkan. 1994. Combined refraction/diffraction model for spectral wave conditions, REF/DIF S, Version 1.1, Documentation and User's Manual, Research Report, Center for Applied Coastal Research. University of Delaware, Newark, Delaware.

Kobayashi, N., A. W. Raichle, and T. Asano. 1993. Wave attenuation by vegetation. *Journal of Waterway Port Coastal and Ocean Engineering-ASCE* 119:30–48.

Koch, E. W. 1993. Hydrodynamics of flow through seagrass canopies. Ph.D. Dissertation, University of South Florida, St. Petersburg, Florida.

Koch, E. W. 1996. Hydrodynamics of a shallow *Thalassia testudinum* bed in Florida, USA, p. 105–110. *In* J. Kuo, R. C. Phillips, D. I. Walker, and H. Kirkman (eds.), Seagrass Biology – Proceedings of an International Workshop, Western Australia Museum, Perth, Australia.

Koch, E. W. 2001. Beyond light: Physical, geological and geochemical parameters as possible submersed aquatic vegetation habitat requirements. *Estuaries* 24:1–17.

Koch, E. W., J. D. Ackerman, and J. Verduin. 2006. Fluid dynamics in seagrass ecology: From molecules to ecosystems, p. 193–225. *In* A. W. D. Larkum, R. J. Orth, and C. M. Duarte (eds.), Seagrasses: Biology, Ecology and Conservation, Volume 1. Springer Verlag, New York.

Kundu, P. K. and I. M. Cohen. 2002. Fluid Mechanics, 2nd edition. Academic Press, San Diego, California.

Leonard, B. P. 1979. Stable and accurate convective modeling procedure based on quadratic upstream interpolation. *Computer Methods in Applied Mechanics and Engineering* 19:59–98.

Lopez, F. and M. Garcia. 1998. Open-channel flow through simulated vegetation: Suspended sediment transport modeling. *Water Resources Research* 34:2341–2352.

Mendez, F. J. and I. J. Losada. 2004. An empirical model to estimate the propagation of random breaking and nonbreaking waves over vegetation fields. *Coastal Engineering* 51:103–118.

Mendez, F. J., I. J. Losada, and M. A. Losada. 1999. Hydrodynamics induced by wind waves in a vegetation field. *Journal of Geophysical Research-Oceans* 104:18383–18396.

Nepf, H. M. 1999. Drag, turbulence and diffusion in flow through emergent vegetation. *Water Resources Research* 35:479–489.

Nepf, H. M. and E. R. Vivoni. 2000. Flow structure in depth-limited, vegetated flow. *Journal of Geophysical Research* 105: 28547–28557.

Newell, R. I. E. and E. W. Koch. 2004. Modeling seagrass density and distribution in response to changes in turbidity stemming from bivalve filtration and seagrass sediment stabilization. *Estuaries* 27:793–806.

North, E. W., S. Y. Chao, L. P. Sanford, and R. R. Hood. 2004. The influence of wind and river pulses on an estuarine turbidity maximum: Numerical studies and field observations in Chesapeake Bay. *Estuaries* 27:132–146.

Rybicki, N. B., H. L. Jenter, V. Carter, R. A. Baltzer, and M. Turtora. 1997. Observations of tidal flux between a submersed aquatic plant stand and the adjacent channel in the Potomac River near Washington, D.C. *Limnology and Oceanography* 42: 307–317.

Sanford, L. P., S. E. Suttles, and J. P. Halka. 2001. Reconsidering the physics of the Chesapeake Bay estuarine turbidity maximum. *Estuaries* 24:655–669.

SCOFFIN, T. P. 1970. The trapping and binding of subtidal carbonate sediments by marine vegetation in Bimini Lagoon, Bahamas. *Journal of Sedimentary Petrology* 40:249–273.

SHI, F., I. A. SVENDSEN, J. T. KIRBY, AND J. M. SMITH. 2003. A curvilinear version of a Quasi-3D nearshore circulation model. *Coastal Engineering* 49:99–124.

SVENDSEN, I. A., K. HAAS, AND Q. ZHAO. 2000. Quasi-3D nearshore circulation model, SHORECIRC, Version 1.3.6, Documentation and User's Manual, Center for Applied Coastal Research. University of Delaware, Newark, Delaware.

TEETER, A. M. 2001. Sediment resuspension and circulation of dredged material in Laguna Madre, Texas. Technical Report, U.S. Army Engineer Research and Development Center, Vicksburg, Mississippi.

TEETER, A. M., B. H. JOHNSON, C. BERGER, G. STELLING, N. W. SCHEFFNER, M. H. GARCIA, AND T. M. PARCHURE. 2001. Hydrodynamic and sediment transport modeling with emphasis on shallow-water, vegetated areas (lakes, reservoirs, estuaries and lagoons). *Hydrobiologia* 444:1–24.

U.S. ARMY CORPS OF ENGINEERS. 2002. Coastal Engineering Manual. Engineer Manual 1110-2-1100, U.S. Army Corps of Engineers, Washington, D.C.

VAN KATWIJK, M. M. AND D. C. R. HERMUS. 2000. Effects of water dynamics on *Zostera marina*: Transplantation experiments in the intertidal Dutch Wadden Sea. *Marine Ecology Progress Series* 208: 107–118.

WANLESS, H. R. 1981. Fining upwards sedimentary sequences generated in seagrass beds. *Journal of Sedimentary Petrology* 51: 445–454.

WARD, L. G., W. M. KEMP, AND W. E. BOYNTON. 1984. The influence of waves and seagrass communities on suspended particulates in an estuarine embayment. *Marine Geology* 59:85–103.

WIGAND, C., J. C. STEVENSON, AND J. C. CORNWELL. 1997. Effects of different submersed macrophytes on sediment biogeochemistry. *Aquatic Botany* 56:233–244.

WILCOCK, P. R., D. S. MILLER, R. H. SHEA, AND R. T. KERKIN. 1998. Frequency of effective wave activity and the recession of coastal bluffs: Calvert Cliffs, Maryland. *Journal of Coastal Research* 14: 256–268.

Received, June 27, 2006
Accepted, November 15, 2006